Detailed balance description of energetic photons in heavy-ion collisions

M. Prakash, P. Braun-Munzinger, and J. Stachel
Physics Department, State University of New York at Stony Brook, Stony Brook, New York 11794

N. Alamanos
Centre d'Etudes Nucléaires de Saclay, Service de Physique Nucléaire a Basse Énergie, Saclay, F-91191, Gif-sur-Yvette, Cedex, France

(Received 22 December 1987)

Photon production cross sections in intermediate energy heavy-ion reactions are calculated using detailed balance. The model gives substantial photon yields and reproduces qualitatively the experimental observations. A possible influence of the Δ-isobar degree of freedom on the high energy photon yield is pointed out.

Many experimental groups have recently investigated high energy photon production in intermediate energy (20 MeV $< E_{\rm lab}/A <$ 100 MeV) heavy-ion collisions. Different mechanisms have been suggested for the photon emission process.[1-10] For example, these include coherent nucleus-nucleus bremsstrahlung, nucleon bremsstrahlung in the nuclear potential field, and bremsstrahlung from individual neutron-proton collisions. The majority of these approaches are based on the mechanism of photon emission in nucleon-nucleon collisions during the very early stages of the reaction. Hard collisions between the nucleons of the colliding nuclei, however, tend to randomize the momentum distributions as the interpenetration progresses. Thus contributions to photon yields from a nearly thermalized source are also to be expected.

Here we calculate the thermal contribution using an approach that employs detailed balance. Such a description[11-15] has proved useful in understanding qualitatively many features of pion production close to the absolute threshold. Since this approach does not make use of the soft photon approximation, one can extend the calculations to emitted photon energies of several hundreds of MeV and thereby investigate a possible influence of the Δ-isobar degree of freedom.

We assume that during the collision the overlapping projectile and target matter form a composite system with a volume and a temperature depending on the impact parameter b. The numbers of participating projectile and target nucleons are determined from the volume of intersection of two rigid spheres each with uniform density ρ_0. Details about the geometry may be found in Ref. 16 and in Ref. 14, where pion production close to threshold was investigated. The model is extended here to study photon emission. For beam energies approaching the lower limit of the range considered here, the above geometrical procedure is somewhat oversimplified. Our purpose, however, is to provide a benchmark calculation that exemplifies the use of detailed balance. Comparisons with more realistic and necessarily more involved calculations will then provide additional insight into aspects of dynamics and approach to equilibrium not considered here.

Note that produced particles like pions and photons are not required to be in equilibrium with the constituents of this composite system. Particle or photon production cross sections are thus governed by the available phase space and rates determined from detailed balance. The inclusive photon production cross section is then given by

$$\sigma_\gamma = \int_0^{b_{\max}} 2\pi b\, db \int \frac{W_{if}(b,E)}{\sum_j \int W_{ij}(b,E_j)dE_j} dE \ , \qquad (1)$$

where E is the energy of the emitted particle or photon and $W_{if}(b,E)$ represents the transition rate at impact parameter b and for energy E of the emitted particle or photon. The summation index j stands for the emitted particle species. The limit $b_{\max}$ is determined from physical considerations (see below).

The basic formula for the transition rate is given by[17]

$$W_{if}(b,E)dE = \frac{g}{2\pi^2\hbar^3}\frac{\rho[U(b)]}{\rho[E_{\rm ex}(b)]}\sigma_{fi}(b,E)p^2 dE \ . \qquad (2)$$

The factor g accounts for the total number of intrinsic degrees of freedom. For particles, $g=(2s+1)$, where s is the intrinsic spin. For photons, $g=2$ from the two (normally not measured) polarizations. The function ρ describes, in the rest frame of the decaying system, the level densities of the initial and final states of the composite system at excitation energies $E_{\rm ex}(b)$ and $U(b)$, respectively. $\sigma_{fi}(b,E)$ is the inverse cross section at energy E of the emitted particle (or of the photon) and p is the momentum.

The denominator in (1) is calculated by considering only nucleon and photon emission. At the excitation energies of interest here α particle emission may still be relevant but its inclusion is mostly expected to reduce somewhat the overall magnitude of the calculated cross section. Photon yields are then computed as the sum of contributions from a cascade that conserves energy on the average.

The central ingredient in (2) is the inverse cross section σ_{fi} for photoabsorption on nuclei. We therefore discuss photoabsorption cross sections in some detail.

PHOTOABSORPTION CROSS SECTIONS

Fortunately, good quality data for photoabsorption on nuclei ranging from Li to Pb in their ground state are available.[18] Absorption cross sections per nucleon are found to be nearly independent of target mass. For details of current understanding from a theoretical standpoint we refer the reader to the reviews in Refs. 19–22 (we will discuss later the influence of finite temperature on absorption cross sections). In Fig. 1, a sample of the measured photoabsorption cross sections per nucleon as a function of incident photon energy is shown by the dots. Three distinct regions may be observed.

(1) The giant resonance region ($E_\gamma < 40$ MeV). Here the photon is mainly absorbed in dipole transitions either through direct or through resonant channels. The Lorentzian parametrization of the classical photoabsorption ($L=1$) sum rule

$$\sigma_{GD}(E_\gamma)=\frac{60NZ}{A}\frac{2}{\pi\Gamma_1}\frac{(\Gamma_1 E_\gamma)^2}{(\Gamma_1 E_\gamma)^2+(E_\gamma^2-E_R^2)^2}\ \text{mb}\ , \quad (3)$$

with $\Gamma_1=6$ MeV and $E_R=34A^{-1/6}$ MeV reproduces the gross features of the data. N, Z, and A are, respectively, the number of neutrons, protons and the mass number of the composite system.

(2) The quasideuteron region ($50<E_\gamma<140$ MeV). The cross section is a slowly decreasing function of energy and is due to the interaction of a photon with a pair of nucleons, i.e., a quasideuteron. An estimate of the photoabsorption cross section in this energy range can be obtained by[23]

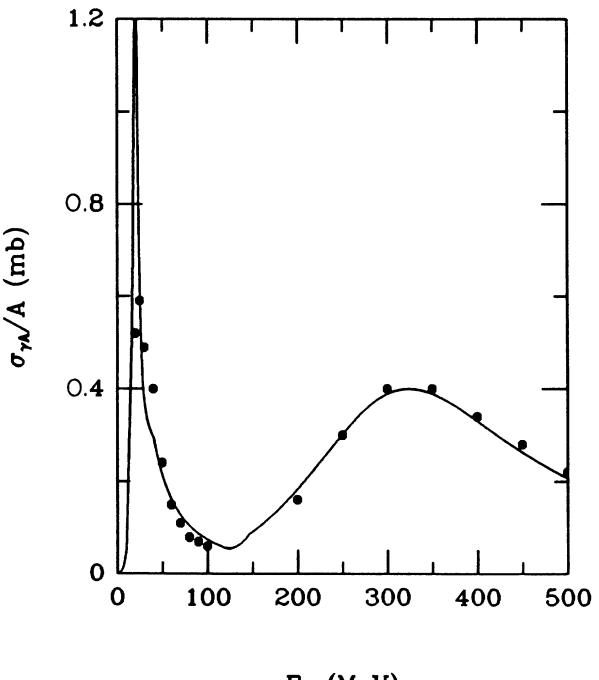

FIG. 1. Photon absorption cross section per nucleon as a function of incident photon energy. The dots show representative data points from Ref. 18. The solid curve is obtained from a smooth fit using Eqs. (3)–(5) (see text for details).

$$\sigma_{QD}(E_\gamma)=300\frac{NZ}{A}E_\gamma^{-3/2}f_{PB}(E_\gamma)\ \text{mb}\ . \quad (4)$$

The function $f_{PB}(E_\gamma)$ accounts for Pauli blocking of the final state nucleons which becomes progressively stronger as the photon energy is decreased below twice the Fermi energy E_F. It is phenomenologically accounted[21,23] for by a function of the form $\exp(-D/E_\gamma)$ with $D=(60-80)$ MeV. Here we use an interpolating procedure to best fit the data.

(3) The Δ-isobar region ($140<E_\gamma<500$ MeV). Above the pion threshold, absorption is dominated by the transition to the first excited state of the nucleon, the Δ resonance. The data can be fitted with a Lorentzian

$$\sigma_\Delta(E_\gamma)=0.4A\frac{(\Gamma_2 E_\gamma)^2}{(\Gamma_2 E_\gamma)^2+(E_\gamma^2-E_R^2)^2}\ \text{mb} \quad (5)$$

using $\Gamma_2=300$ MeV and $E_R=(2.1m_\pi+30)$ MeV.

For $0<E_\gamma<500$ MeV, the photoabsorption cross section $\sigma_{\gamma A}/A$ is calculated from (3)–(5) by joining smoothly the cross sections per nucleon at the energies connecting the different regions. The solid curve in Fig. 1 shows our fit to the data. Since the measured photoabsorption cross section does not strictly scale with A in the vicinity of the isovector giant resonance ($L=1$), a good agreement between the data and the fit is not expected at low energies. For $E_\gamma>40$ MeV, the absorption cross sections per nucleon are almost the same for all nuclei within experimental uncertainties.

For nucleons the inverse cross section is taken to be the geometric absorption cross section.

PHOTOABSORPTION ON EXCITED NUCLEI

The discussion above refers to γ absorption on nuclei in their ground state. Note, however, that (2) requires inverse cross sections for systems with considerable excitation energies. The resulting high temperatures are expected to alter significantly the cross section for absorption in the giant dipole resonance region.[24] We are, however, interested only in the energy region above $E_\gamma=50$ MeV, i.e., in the quasideuteron and the Δ-resonance regions. We consider now these two regions in turn.

(i) The quasideuteron region. Relation (4) is based on γ absorption on a pair of nucleons. For $E_\gamma>2E_F$, Pauli blocking of final states is absent and Levinger's original formulation[23] may be used. Explicitly,

$$\sigma_{QD}(E_\gamma)=\sigma_D(E_\gamma)\frac{NZ}{A}\left[\frac{2\pi(1-\alpha r_0)}{(4\pi r_0^3/3)\alpha}\langle\alpha^2+k^2\rangle_{av}^{-1}\right], \quad (6)$$

where σ_D is the γ-absorption cross section on a deuteron,

$$\alpha^{-1}=[\hbar^2/(2.23M_N)]^{1/2}$$

is the deuteron scattering length (M_N is the nucleon mass), and $r_0\cong(1.3-1.4)$ fm. The averaging is performed over all possible values of the relative momenta k for a pair of nucleons in a Fermi gas. Retaining the picture of γ absorption on a pair of nucleons, an estimate for

σ_{QD} at finite temperature is obtained by using the thermal average

$$\langle \alpha^2+k^2\rangle_{av}^{-1}(T) = \int\int d\mathbf{k}_1 d\mathbf{k}_2 P(\mathbf{k}_1,T)P(\mathbf{k}_2,T)(\alpha^2+k^2)^{-1} \quad (7)$$

in (6). In (7), $P(\mathbf{k}_{1,2},T)$ are Fermi-Dirac functions each normalized to unity. After performing the angular integrations in (7), we obtain

$$\langle \alpha^2+k^2\rangle_{av}^{-1}(T)=\int_0^\infty dk\, N(k,T)(\alpha^2+k^2)^{-1}\,, \quad (8)$$

with

$$N(k,T)=\left[\frac{2}{\rho_0\pi^2}\right]^2 k^2\int_0^\infty dK \frac{K^2}{e^{2a-1}} \times\left\{1+\ln\left[\frac{1+e^{-(a+b)}}{1+e^{(a+b)}}\right]\right\}. \quad (9)$$

Here $2\mathbf{k}=\mathbf{k}_1-\mathbf{k}_2$, $\mathbf{K}=\mathbf{k}_1+\mathbf{k}_2$, and

$$a=\frac{\hbar^2}{2mT}\left[\frac{K^2}{4}+k^2\right]-\frac{\mu}{T}$$

and

$$b=\frac{\hbar^2}{2mT}Kk\,.$$

The function $N(k,T)$ gives the probability density for the relative momentum k of a pair of particles and is shown in Fig. 2 for $T=0$ and $T=20$ MeV, respectively. The magnitude of mean relative momentum at $T=20$ MeV is $\sim 0.63k_F$, only slightly larger than $\sim 0.51k_F$ for the zero temperature case (unless otherwise stated we use $\rho_0=0.15$ fm^{-3} or $k_F\cong 1.31$ fm^{-1} throughout). The magnitude of $\langle \alpha^2+k^2\rangle_{av}^{-1}(T)$ in (6) is determined largely by the magnitude of $N(k,T)$ for momentum values less than the above mean momenta. As the probabilities for finite T are in general smaller than for $T=0$, the corresponding σ_{QD} are also smaller.

In Fig. 3 we show $\langle \alpha^2+k^2\rangle_{av}^{-1}(T)/\langle \alpha^2+k^2\rangle_{av}^{-1}(0)$ as a function of temperature. At $T=15$ (20) MeV, this ratio is 0.75 (0.66). Finite temperatures thus reduce σ_{QD} by at most 30% at the largest beam energy of interest here. In discussing our results later we will take this into consideration in the form of a downward correction factor.

The density dependence of $\langle \alpha^2+k^2\rangle_{av}^{-1}(0)$ is governed largely by terms of $\mathcal{O}(k_F^{-2})$. More precisely, $\langle \alpha^2+k^2\rangle_{av}^{-1}(0)=3.95$, 2.86, and 2.02 fm^2 for $\rho=0.5\rho_0$, ρ_0 and $2\rho_0$, respectively. The corresponding values at $T=20$ MeV are $\langle \alpha^2+k^2\rangle_{av}^{-1}(T)=2.11$, 1.89, and 1.58 fm^2, respectively. At the bombarding energies of interest here it is unlikely that a significant compression of matter is attained. Our choice of $\rho_0=0.15$ fm^{-3} is thus to be thought of as a reasonable representative value for the density of the composite system.

For $E_\gamma<2E_F$ and for $T=0$, Pauli blocking of final states for the neutron and/or proton suppresses the absorption process relative to that given by (6). For photon energies of interest here ($E_\gamma>50$ MeV), the relevant range to consider is $\frac{1}{2}\le\hat{E}_\gamma\le 1$ with $\hat{E}_\gamma=E_\gamma/2E_F$. In this range the distribution for the initial state relative momentum k is given by[25]

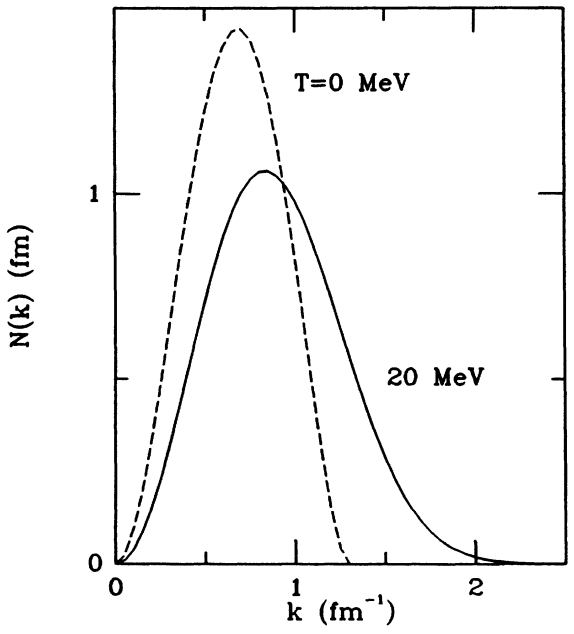

FIG. 2. The probability density distribution from Eq. (9) for the relative momentum k of a pair of nucleons inside a nucleus. The dashed (solid) curve is for a nuclear temperature of $T=0$ (20) MeV.

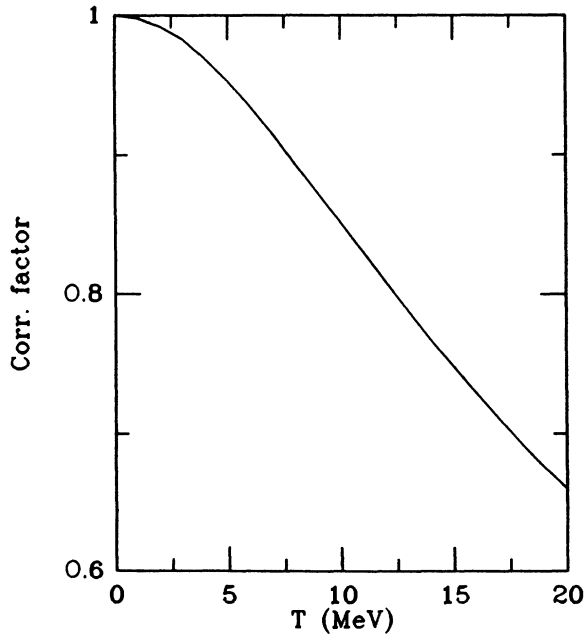

FIG. 3. The ratio $\langle \alpha^2+k^2\rangle_{av}^{-1}(T)/\langle \alpha^2+k^2\rangle_{av}^{-1}(0)$ as a function of temperature (see text).

$$N_{\rm PB}(k,0)=\begin{cases} N(k,0)-\left[1-\hat{E}_\gamma-\left[\dfrac{k}{k_F}\right]^2\right]^{3/2}, \\ \qquad k/k_F\le(1-E_\gamma)^{1/2} \\ N(k,0), \quad k/k_F\ge(1-E_\gamma)^{1/2} \end{cases} \tag{10}$$

where

$$N(k,0)=\frac{24}{k_F}\left[\frac{k}{k_F}\right]^2\left[1-\frac{3}{2}\left[\frac{k}{k_F}\right]+\frac{1}{2}\left[\frac{k}{k_F}\right]^3\right] \tag{11}$$

is the probability density in (9) at $T=0$. The distribution $N_{\rm PB}(k,0)$ differs significantly from $N(k,0)$ only for E_γ approaching the lower limit of the range considered. We recall that in our fit to the data [see (4)] full account of Pauli effects is already contained. Such a hindrance is less severe at finite temperatures due to the availability of partially filled states. Thus $\sigma_{\gamma A}$ at finite temperatures is somewhat enhanced relative to the $T=0$ case. Rather than using such enhancements due to effects of finite temperature in this energy range, we shall use the results of Fig. 3 and an overall reduction factor in our total γ-production cross sections. This procedure should underestimate slightly the magnitude of γ emission from this source.

(ii) The Δ-resonance region. Compared to the γ-nucleon absorption cross section ($\sigma_{\gamma N}$) in this region, the γ-nucleus cross sections per nucleon ($\sigma_{\gamma A}/A$) show two distinct features.[18,19] Firstly, the half-width for the latter is somewhat larger (with reduced peak cross sections) than for $\sigma_{\gamma N}$. Secondly, the peak position is shifted slightly upward. For the most part, the first of these two features is understood as due to the Fermi motion of target nucleons while the second feature is due to binding energy effects. For details on other medium-dependent effects see the review articles in Refs. 19–22. To illustrate the changes brought about by finite temperature in the γ-absorption cross sections, we will concentrate on the effects due to Fermi motion. We follow closely the isobar doorway state approach of Ref. 20 in which near resonance the dominant contribution from the coupling to the second doorway state is an increase in the half-width

$$\delta(\Gamma/2)=\frac{\mathcal{H}_{01}\mathcal{H}_{10}}{\Gamma/2}=\frac{\langle\mathcal{H}^2\rangle_{00}-\langle\mathcal{H}\rangle_{00}^2}{\Gamma/2}=\frac{\langle\delta\mathcal{H}^2\rangle_{00}}{\Gamma/2}, \tag{12}$$

where $\mathcal{H}_{\Delta h}$ is the isobar-hole Hamiltonian in medium. We can estimate the size of this effect by evaluating the fluctuation in a Fermi gas at finite temperature:

$$\langle\delta T_\Delta^2\rangle=\int d\mathbf{k}\,P(\mathbf{k},T)[\Delta_{\mathbf{k}+\mathbf{p}_\gamma}-\epsilon_{\mathbf{k}}]^2 - \left[\int d\mathbf{k}\,P(\mathbf{k},T)[\Delta_{\mathbf{k}+\mathbf{p}_\gamma}-\epsilon_{\mathbf{k}}]\right]^2, \tag{13}$$

where, as in (7), $P(\mathbf{k},T)$ is the Fermi-Dirac occupation factor and

$$\epsilon_{\mathbf{k}}=M_{\rm N}+\frac{k^2}{2M_{\rm N}}$$

and

$$\Delta_{\mathbf{k}+\mathbf{p}_\gamma}=M_\Delta+\frac{(\mathbf{k}+\mathbf{p}_\gamma)^2}{2M_\Delta}.$$

After performing the angular integrations involving $\mathbf{k}\cdot\mathbf{p}_\gamma$ in (13), we find

$$\langle\delta T_\Delta^2\rangle=\left[\frac{M_\Delta-M_{\rm N}}{M_\Delta}\right]^2\left[\int d\mathbf{k}\,P(\mathbf{k},T)\left[\frac{k^2}{2M_{\rm N}}\right]^2 - \left[\int d\mathbf{k}\,P(\mathbf{k},T)\frac{k^2}{2M_{\rm N}}\right]^2\right] + \frac{4M_{\rm N}}{3}\frac{p_\gamma^2}{M_\Delta^2}\int d\mathbf{k}\,P(\mathbf{k},T)\frac{k^2}{2M_{\rm N}}. \tag{14}$$

Near resonance, i.e., $p_\gamma\cong(M_\Delta-m_{\rm N}+30)$ MeV, the dominant contribution to (14) comes from the second term. This term has an explicit k_F^2 dependence and reflects the density dependence of the increase in the half-width. In Table I, results for the increase in the half-width are shown for several values of temperature and for $k_F\cong1.04$ fm^{-1} and $k_F\cong1.31$ fm^{-1}. The associated decrease in the peak cross sections are listed in the last column.

The increase in the half-width has the effect of enhancing the γ-absorption cross sections close to the pion threshold relative to the zero temperature case. The peak cross sections are reduced correspondingly. While these

TABLE I. Results from Fermi broadening of the Δ resonance for incident $p_\gamma\cong(M_\Delta-M_{\rm N}+30)$ MeV. The second column gives increase in the half-width from 75 MeV for $p_\gamma=324$ MeV. The last column gives the decrease in the peak cross section.

T (MeV)	$\delta(\Gamma/2)$ (MeV)	$\delta(\sigma_\Delta)$ (%)	T (MeV)	$\delta(\Gamma/2)$ (MeV)	$\delta(\sigma_\Delta)$ (%)
	$k_F\cong1.04$ fm^{-1}			$k_F\cong1.31$ fm^{-1}	
0	7.3	−9.8	0	11.7	−15.5
5	8.7	−11.7	5	16.8	−16.8
10	11.8	−15.8	10	20.1	−20.1
15	15.5	−20.7	15	24.5	−24.5
20	19.5	−26.0	20	29.3	−29.3

changes do not affect significantly the total γ-production cross sections, they are important if the possible influence of the Δ resonance on photon production is investigated.

RESULTS AND DISCUSSION

To compare the results of our calculations with the available data,[26–33] we have collected in Table II most of the reactions investigated below 85 MeV per nucleon beam energy. Source velocities, slope parameters of the differential cross sections, and total cross sections for $E_\gamma > 50$ MeV are then listed in order.

The calculated source velocities $\langle \beta_{\text{c.m.}} \rangle$ are averaged over the impact parameter b and are in good agreement with those extracted from the data. This agreement lends some support to the geometrical concepts of the model and the kinematics of the source from which photons are emitted. Since the mass of the composite system is generally more than twice the projectile mass for reactions involving unequal masses, results for $\langle \beta_{\text{c.m.}} \rangle$ are slightly smaller than the velocity of the nucleon-nucleon center of mass.

For each impact parameter b, the differential spectra in the laboratory and the c.m. systems are related through

$$\frac{d^2\sigma}{dE_{\text{lab}}d\Omega_{\text{lab}}} = \left[\frac{p_{\text{lab}}}{p_{\text{c.m.}}}\right] \frac{d^2\sigma}{dE_{\text{c.m.}}d\Omega_{\text{c.m.}}} \tag{15}$$

with $E_{\text{c.m.}} = \gamma_{\text{c.m.}}[E_{\text{lab}} - \beta_{\text{c.m.}} p_{\text{lab}} \cos(\theta_{\text{lab}})]$. One can use $\langle \beta_{\text{c.m.}} \rangle$ in place of $\beta_{\text{c.m.}}$ without much loss in accuracy since the latter is a slowly varying function of b. We shall adopt this procedure when comparing the calculated laboratory differential spectra with those measured. The magnitudes of $\beta_{\text{c.m.}}$ shown in Table II are small enough that the angle integrated spectral distributions do not differ much between the laboratory and c.m. systems.

For photon energies well above the giant resonance region and up to the maximum energy measured so far, the photon yields decrease roughly like $\exp(-E_\gamma/E_0)$. The slope constant E_0 listed in the table was obtained from the calculated differential cross sections in the energy range 50 MeV $< E_\gamma <$ 100 MeV. Most of the experimental slopes given in the table also refer to $E_\gamma > 50$ MeV and for $\theta_{\text{lab}} = 90°$. On the average the calculated slopes are slightly smaller than experimentally observed. This is reminiscent of similar trends encountered in pion production close to threshold.[14]

TABLE II. Comparison of calculated and experimental results. Photon source velocities are in units of the velocity of light. Slope parameters E_0 are extracted from the $50 < E_\gamma < 100$ MeV region. Integrated cross sections shown are for $E_\gamma > 50$ MeV in the laboratory system. Where possible experimental cross sections have been corrected for detector response.

Reaction	ϵ_{lab} (MeV)	$\langle \beta_{\text{c.m.}} \rangle$	$\langle \beta_{\text{c.m.}} \rangle$(expt)	E_0 (MeV)	E_0(expt) (MeV)	σ_γ (μb)	σ_γ(expt) (μb)	Ref.
$^{12}C+^{12}C$	48	0.16		10.6	19±1.5	36	38±9	26
	60	0.18	0.18±0.02	13.2	20±1.5	67	60±13	
	74	0.20	0.20±0.02	15.7	23±1.5	108	100±17	
	84	0.21	0.21±0.02	17.2	27±1.5	138	160±35	
$^{86}Kr+^{12}C$	44	0.19	0.17±0.01	10.5	11.6±0.5	205	55±10	31
$^{86}Kr + Ag$	44	0.15	0.18±0.01	12.9	12.5±0.3	2730	450±60	
$^{86}Kr+^{197}Au$	44	0.14	0.14±0.01	12.7	12.1±0.2	4773	440±35	
$^{12}C + Sn$	84	0.16		17	25±1	1131		
$^{40}Ar + Ge$	15	0.08		6.3	4.0	26		
	24	0.11		8.4	6.5	143		
$^{14}N + Ni$	35	0.11		9.3	13.5±1	91	50±15	27
$^{40}Ar+^{158}Gd$	44	0.13	0.24±0.1	11.7	12.6±0.6	1532	400±200	30
$^{40}Ar+^{197}Au$	30	0.10	0.12	9.4	7.5	663	50±20	29
$^{32}S+^{27}Al$	22	0.11		7.4	10.8±1	29	35±17	33
$^{32}S + Ni$	22	0.10		7.8	10.0±1	67	60±30	
$^{32}S+^{197}Au$	22	0.09		7.7	9.1±1	188	91±45	
$^{14}N+^{208}Pb$	20	0.07	0.08	6	10.0	34	7.2	28
	30	0.09	0.11	8.2	12	150	39	
	40	0.10	0.10	9.8	14.2	350	150	
$^{14}N+^{12}C$	20	0.11	0.08	4.9	7.7	1.7	1.2	
	30	0.13	0.10	7.5	11.1	10	7.2	
	40	0.15	0.12	9.5	13.3	26	20	
$^{16}O + W$	15	0.07		5	6±1	10	0.07	32
$^{16}O+^{58}Ni$	44	0.13		10.9		201		Fig. 6
	95	0.19		19.5		1142		

The calculated energy spectra for $\theta_{lab}=90°$ are compared with the experimental spectra for the reactions $^{32}S+^{197}Au$ at 22 MeV per nucleon and $^{86}Kr+^{12}C$ at 44 MeV per nucleon in Figs. 4 and 5, respectively. Good qualitative agreement with the data is obtained. The rate of exponential fall off may be understood by examining the energy-dependent factors in (2) for the transition rate. The factors involving the level density give rise to the $\sim\exp(-E_\gamma/T)$ behavior, where T is the temperature of the composite system. For $0<E_\gamma<140$ MeV, the inverse cross section falls off like $E_\gamma^{-3/2}$. As a result the slope constant E_0 is slightly less than T in the energy range considered. This innate feature of the model applies to all systems considered and for photon energies below the photo-pion threshold. For the spectrum in Fig. 4, $T=8.4$ [9.4] MeV for impact parameter $b=0$ [$0.8\times(R_P+R_T)$] while the slope constant $E_0=7.7$ MeV. This is reasonably close to the slope constant 9.1 ± 1 MeV of the experimental spectrum. For the spectrum in Fig. 5, $T=12.5$ [14.2] MeV for $b=0$ [$0.8\times(R_P+R_T)$] while the slope constant $E_0=10.5$ MeV. This is to be compared with $E_0=11.6\pm0.5$ MeV of the experimental spectrum.

The calculated total cross sections for photon emission shown in Table II also refer to $E_\gamma>50$ MeV. Likewise the experimental data. Effects of temperature-dependent absorption cross sections have been incorporated in the quoted γ-production cross sections. For reactions with equal masses, the temperature T remains constant as a function of impact parameter. In the case of asymmetric systems T increases only slightly with impact parameter.[14] Results from Fig. 3 therefore serve as downward correction factors to cross sections calculated with the zero temperature γ-absorption cross sections. As yields in the Δ-resonance region are down by about an order of magnitude compared to those in the QD region, they do not contribute significantly to the total γ-production cross sections. For many cases, the calculated cross sections are somewhat larger than the data. For intermediate mass systems, the discrepancy between the model and the data is more marked. One should, however, exercise some caution in interpreting agreement or lack thereof by comparing the calculated and experimental cross sections integrated above some threshold value, e.g., $E_\gamma=50$ MeV. A direct comparison is meaningful only when the slope constants of the calculated spectra agree with those measured. Our calculations systematically underpredict slope constants. Results for integrated cross sections depend on both the threshold chosen and the slope constant and therefore can be used only to make qualitative statements when comparing with the data. The important point, however, is that a substantial part of the observed cross sections could stem from thermal sources.

Note that the model assumes full stopping, viz., all the beam energy is utilized in heating the participant nucleus. It is likely that the fireball geometry overestimates the number of participant nucleons. If a smaller number of nucleons were to constitute the source of photon emission, smaller cross sections than shown would be obtained since the inverse γ cross sections scale with nucleon number. Concomitantly, the temperature of the source would be larger than given by the fireball geometry and higher slope constants would result. The final result would then depend on the interplay between effects associated with the smaller nucleon numbers but larger temperatures.

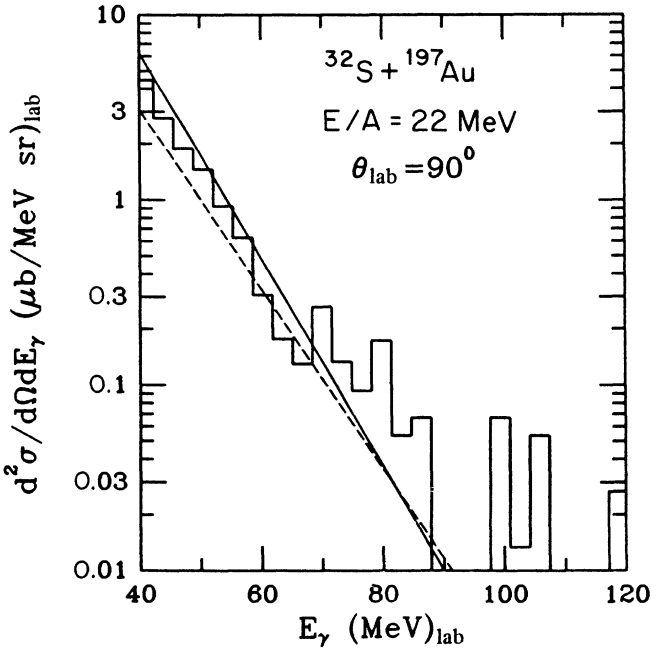

FIG. 4. Comparison of calculated (solid line) and experimental photon differential cross sections in the laboratory system. The histograms are the uncorrected data from Ref. 33. Data corrected for detector response are shown by the dashed lines.

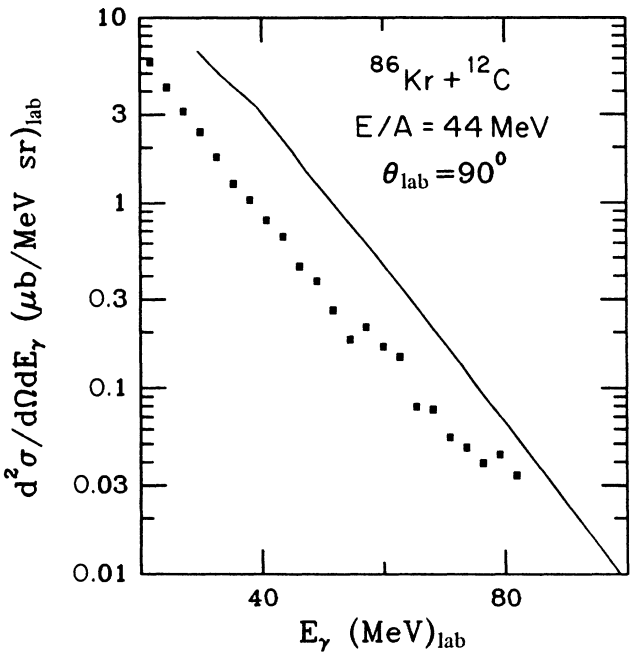

FIG. 5. Comparison of calculated (solid line) and experimental photon differential cross sections in the laboratory system. The data are taken from Ref. 31.

In the present approach, the angular distribution of the emitted photons is isotropic in the rest frame of the hot composite system. No general consensus has yet been reached experimentally about the nature of the photon angular distributions. Some investigators[28,30] report distributions that are isotropic in the nucleon-nucleon center of mass, while others[26,27,31,33] report dipole components of different magnitudes. Such dipole components may be obtained from the present model if angular momentum conservation is taken into account. Note that $k_\gamma R_s \sim 1$ for photon energies and source sizes relevant here.

We turn now to features of photon yields for $E_\gamma > 140$ MeV, i.e., above the photo-pion threshold. Note that the inverse cross sections in Fig. 1 are sizable as a consequence of the Δ-isobar degree of freedom coming into play. To investigate their influence, we have calculated the differential cross section $d\sigma_\gamma/dE_\gamma$ for the system $^{16}O+^{58}Ni$ at energies available in the existing accelerators.

In Fig. 6 the calculated results are shown at $E_{lab}/A = 44$ MeV and $E_{lab}/A = 95$ MeV, respectively. The differential cross sections break away from an exponential decrease for photon energies in excess of ~140 MeV. This feature is more pronounced for the higher beam energy shown in Fig. 6. For photon energies near the peak of the Δ resonance, cross sections are a factor of about 5–10 larger than given by a continuation of the exponential falloff. Up to half the resonance energy, finite temperatures have the effect of enhancing the absorption cross sections due to an increase in the half-width compared to the zero temperature case. Incorporation of such effects will modify the differential cross sections somewhat over those shown in the figure. The possibility to study such effects along with the role of the Δ-isobar degree of freedom in photon production cross sections is intriguing. Observations of an effect from the Δ-isobar

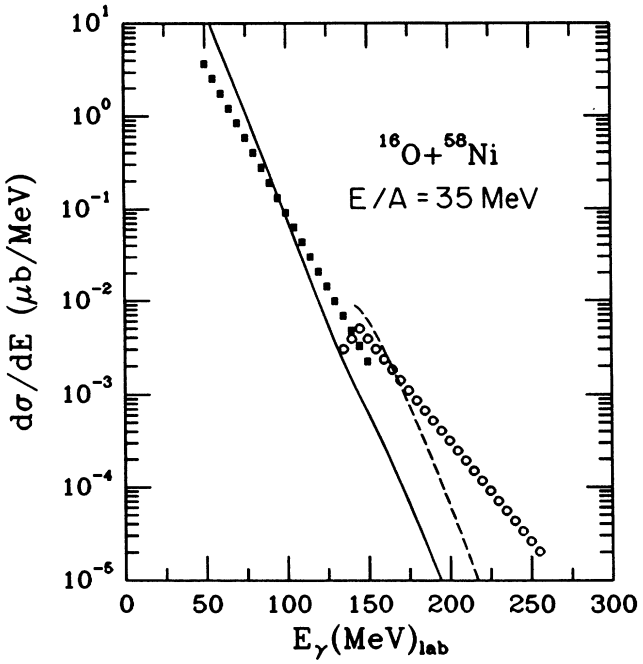

FIG. 7. Comparison of pion (dashed line) and photon (solid line) differential cross sections in the laboratory system. The data are taken from Ref. 27 for photons (solid squares) after correction for detector response and Ref. 34 for pions (open circles).

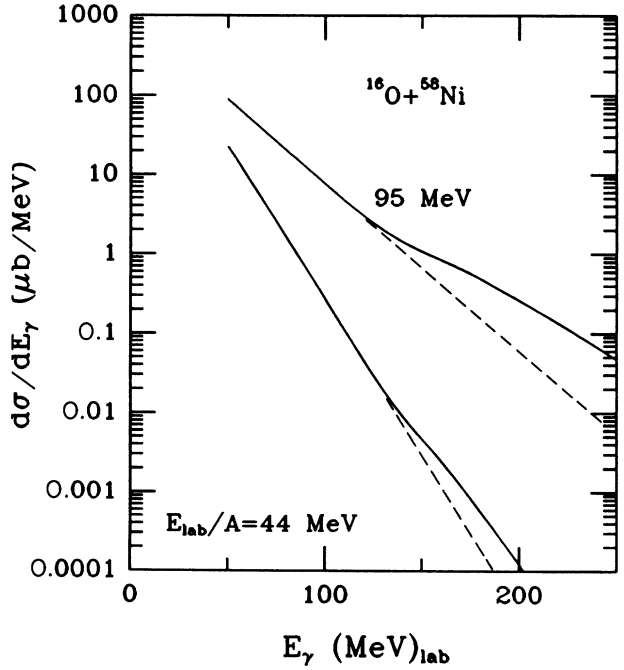

FIG. 6. Calculated photon differential cross sections in the laboratory system. Beyond the photo-pion threshold of 140 MeV, the exponentially falling trend is broken due to the influence of the Δ-isobar degree of freedom.

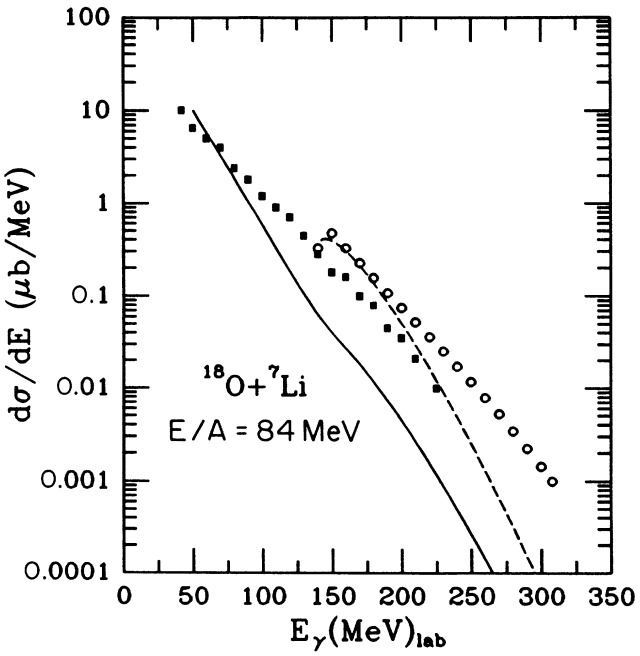

FIG. 8. Comparison of pion (dashed line) and photon (solid line) differential cross sections in the laboratory system. The data are from Ref. 35. Symbol designations for the data are solid squares for photons and open circles for pions.

on photon spectra might provide interesting information about the position and width of the Δ-isobar in hot nuclei. We therefore suggest that accurate photon yield measurements be carried out in this energy range.

We now inquire into the relative yields of photons and pions at the same total energy, i.e., $E_\gamma = E_\pi = m_\pi + T_\pi$. For a fixed excitation energy of the composite system with A particles, Eqs. (1) and (2) yield the simple relation

$$\frac{d\sigma_\pi/dE_\pi}{d\sigma_\gamma/dE_\gamma} = \frac{1}{2}\frac{\sigma_{\pi A}(T_\pi)}{\sigma_{\gamma a}(E_\gamma = m_\pi + T_\pi)}\left[\frac{p_\pi}{p_\gamma}\right]^2 . \quad (16)$$

The numerical factor here arises from the number of intrinsic degrees of freedom for neutral pions and for photons, respectively. Note that the inverse cross sections are to be taken at the same total energy for both photons and pions. This relation holds strictly for a given impact parameter b. Results obtained by using the most probable b are, however, close to those obtained by averaging over b.

In Figs. 7 and 8 the calculated spectral distributions of photons (solid lines) and pions (dashed lines) are compared with those measured[27,34,35] for the systems $^{16}O+^{58}Ni$ at 35 MeV per nucleon and $^{18}O+^{7}Li$ at 84 MeV per nucleon, respectively. Symbol designations for the data are solid squares for photons and open circles for pions. The inverse cross section for neutral pions on nuclei are those used in Ref. 14. At the same total energy, experiments find about an order of magnitude more pions than photons. Our calculations are in qualitative agreement with the data. For both cases shown the calculated ratios are somewhat larger than measured. Note also that for high ejectile energies calculations give a steeper falloff of both pion and photon yields than found in experiments. Nevertheless, it is interesting that a qualitative understanding of the relative yields is obtained by combining the experimentally accessible cross sections with a theoretical analysis that employs detailed balance.

In summary, we have shown that a detailed balance approach gives substantial contributions to photon emission in intermediate energy collisions. The model also predicts that sufficient energy will be made available to make the Δ resonance a viable source of high energy photons. This suggests the desirability of accurate photon yield measurements in this energy range using the existing accelerators. We also find qualitative agreement with the data for the ratio of pion to photon yields at the same total energy of the ejectile using the principle of detailed balance.

ACKNOWLEDGMENTS

We thank Gerry Brown for pointing out the relevance of the isobar doorway states in the γ-absorption cross sections. Helpful discussions with Subal Das Gupta are also acknowledged. We are grateful to H. Nifenecker and J. Stevenson for sending us tables of data. Support for M. Prakash by the Department of Energy under Contract No. DE-AC02-76ER13001 with the State University of New York and for P. Braun-Munzinger and J. Stachel by the National Science Foundation and the A. P. Sloan Foundation (J.S.) are acknowledged.

[1]H. Nifenecker and J. P. Bondorf, Nucl. Phys. **A442**, 478 (1985).
[2]C. M. Ko, G. F. Bertsch, and J. Aichelin, Phys. Rev. C **31**, 2324 (1985).
[3]D. Vasak, Phys. Lett. B **176**, 276 (1986).
[4]K. Nakayama and G. F. Bertsch, Phys. Rev. C **34**, 2190 (1986).
[5]W. Bauer, G. F. Bertsch, W. Cassing, and U. Mosel, Phys. Rev. C **34**, 2127 (1986).
[6]W. Bauer, W. Cassing, U. Mosel, M. Tohyama, and R. Y. Cusson, Nucl. Phys. **A456**, 159 (1986).
[7]R. Shyam and J. Knoll, Nucl. Phys. **A448**, 322 (1986).
[8]T. Stahl, M. Uhlig, B. Müller, W. Greiner, and D. Vasak, Z. Phys. A **327**, 311 (1987), and references therein.
[9]D. Neuhausser and S. E. Koonin, Nucl. Phys. **A462**, 163 (1987).
[10]B. A. Remington, M. Blann, and G. F. Bertsch, Phys. Rev. C **35**, 1720 (1987).
[11]J. Aichelin and G. F. Bertsch, Phys. Lett. **138B**, 350 (1984).
[12]C. Gale and S. Das Gupta, Phys. Rev. C **30**, 414 (1984).
[13]J. Aichelin, Phys. Rev. Lett. **52**, 2340 (1984).
[14]M. Prakash, P. Braun-Munzinger, and J. Stachel, Phys. Rev. C **33**, 937 (1986).
[15]A. Bonasera and G. F. Bertsch, Phys. Lett. B **195**, 521 (1987).
[16]J. Gosset *et al.*, Phys. Rev. C **16**, 629 (1977).
[17]V. F. Weisopf, Phys. Rev. **52**, 295 (1937).
[18]J. Ahrens, Nucl. Phys. **A446**, 229 (1985).
[19]J. M. Laget, in *New Vistas in Electro-Nuclear Physics* (Plenum, New York, 1986).
[20]J. H. Koch, E. J. Moniz, and N. Ohtuska, Ann. Phys. **154**, 99 (1984).
[21]W. M. Alberico, M. Ericson, and A. Molinari, Ann. Phys. **154**, 356 (1984).
[22]W. Weise, Nucl. Phys. **A358**, 163c (1981).
[23]J. Levinger, Phys. Rev. **84**, 396 (1951); Phys. Lett. **82B**, 181 (1979).
[24]J. H. Gordhøje, A. M. Bruce, J. D. Garrett, B. Herskind, D. Bernéoud, M. Maurel, H. Nifenecker, J. A. Piston, P. Perrin, C. Ristori, F. Schussler, A. Braco, and M. Pignanelli, Phys. Rev. Lett. **59**, 1409 (1987).
[25]A. Rietan, Nucl. Phys. **64**, 113 (1965).
[26]E. Grosse, P. Grimm, H. Heckwolf, W. F. J. Müller, H. Noll, A. Oskarson, H. Setlzer, and W. Roesch, Europhys. Lett. **2**, 9 (1986), and references therein.
[27]N. Alamanos, P. Braun-Munzinger, R. H. Freifelder, P. Paul, J. Stachel, T. C. Awes, R. L. Ferguson, F. E. Obenshain, F. Plasil, and G. R. Young, Phys. Lett. B **173**, 392 (1986).
[28]J. Stevenson, K. B. Beard, W. Benenson, J. Clayton, E. Kashy, A. Lampis, D. J. Morrissey, M. Samuel, R. J. Smith, C. L. Tam, and J. S. Winfield, Phys. Rev. Lett. **57**, 555 (1986); and J. Stevenson, private communication.
[29]M. Kwato Njock, M. Maurel, E. Monnand, H. Nifenecker, J. A. Piston, F. Schussler, and D. Barneoud, Phys. Lett. B **173**, 392 (1986).
[30]R. Hingmann, W. Kühn, V. Metag, R. Mühlhans, R. Novotny, A. Ruckelshausen, W. Cassing, H. Emling, R. Kulessa, H. J. Wollersheim, B. Haas, J. P. Vivien, A. Boulley, H. Delagrange, H. Doubre, C. Gregoire, and Y. Schutz, Phys. Rev.

Lett. **58**, 759 (1987).
[31]R. Bertholet, M. Kwato Njock, M. Maurel, E. Monnand, H. Nifenecker, P. Perrin, J. A. Pinston, F. Schussler, D. Barneoud, C. Guet, and Y. Schutz, Nucl. Phys. **A474**, 541 (1987).
[32]G. Breitbach, G. Koch, W. Kühn, V. Metag, R. Novotny, A. Ruckelshausen, H. Ströher, S. Tschesche, and E. Grosse, Gesellschaft für Schwerionenforschung Report 87-1 (1986).
[33]J. Stachel, R. Scharf, P. Braun-Munzinger, L. Waters, N. Alamanos, T. C. Awes, G. R. Young, F. Plasil, and F. E. Obenshain (unpublished).
[34]J. Stachel, P. Braun-Munzinger, R. H. Freifelder, P. Paul, S. Sen, P. DeYoung, P. H. Zhang, T. C. Awes, F. E. Obenshain, F. Plasil, G. R. Young, R. Fox, and R. Ronningen, Phys. Rev. C **33**, 1420 (1986).
[35]E. Grosse, Gesellschaft für Schwerionenforschung Report 10-87, 1987 p. 9.